Corrosion Science 80 (2014) 528–535

Contents lists available at ScienceDirect

Corrosion Science

journal homepage: www.elsevier.com/locate/corsci

Short Communication

Self-healing properties of protective coatings containing isophorone diisocyanate microcapsules on carbon steel surfaces

Wei Wang [a,b,*], Likun Xu [a], Xiangbo Li [a], Yi Yang [a], Enpeng An [a]

[a] State Key Laboratory for Marine Corrosion and Protection, Luoyang Ship Material Research Institute (LSMRI), 149-1 Zhuzhou Road, Laoshan District, Qingdao 266101, PR China
[b] College of Materials Science and Chemical Engineering, Harbin Engineering University, Harbin 150001, PR China

ARTICLE INFO

Article history:
Received 5 June 2013
Accepted 29 November 2013
Available online 5 December 2013

Keywords:
A. Carbon steel
A. Organic coatings
B. EIS

ABSTRACT

Microcapsules containing isophorone diisocyanate (IPDI) were used as self-healing additives in the alkyd varnish coatings (AVCs), and their self-healing performance was evaluated in the case of artificial defects on Q235 steel surfaces, using scanning micro-reference electrode technique and Fourier-transform infrared spectroscopy. Comparison of the micromechanical properties between the water-insoluble self-healing products (polyurethanes) and AVCs indicates that the former significantly enhanced the capability of the scratched crevice to successfully endure outer stress. The electrochemical impedance spectroscopy experiments analysed the different stages in the self-healing process. This study successfully demonstrated the self-healing activity of IPDI-AVCs in protecting steel surfaces.

1. Introduction

Self-healing microcapsules, as the most effective corrosion protective materials, have been investigated intensively over the past decade owing to their ease of synthesis [1–4], environmental stability [5,6], surface modification [7,8], and superior protective property [9–11]. The protective coatings based on these self-healing microcapsules are advantageous over the conventional coatings, because the latter is not very effective in repairing the microcracks in steel and other structures [12–17]. In addition, water is known to influence the corrosion process in steel structures by transporting the chemicals required for electrochemical reactions, and by playing the role of reaction solvent. Hence, an effective protective coating, in principle, should be able to stop water from entering the microcracks in the self-healing process. Chemicals containing isocyanate functional groups are easy to react with water (or even water vapour in the air), which can be utilized as potential catalyst-free healing agents in humid/wet environments. The encapsulation of isophorone diisocyanate (IPDI) [18] and hexamethylene diisocyanate (HDI) [19], as self-healing agents, were successfully carried out by the interfacial polymerization of diisocyanate prepolymers and 1,4-butanediol. The self-healing ability of the protective coatings with embedded organic materials such as HDI microcapsules has been demonstrated; however, the mechanism of the self-healing process has not yet been clearly understood.

Furthermore, nanoindentation is an important method for evaluating micromechanical properties of thin films and micro-scale materials [20–23]. The micromechanical behaviour of self-healing epoxy and hardener-loaded microcapsules with poly (melamine–formaldehyde) (PMF) as the shell material has been investigated by nanoindentation tests [24]. The PMF shell material was found to behave as a viscoelastic plastic material. Also, oxygen-plasma-treated carbon nanotubes have been embedded into microcapsules to improve their micromechanical behaviour [25]. Although, a tensile test is generally used in large-scale testing of self-healing abilities [26–28]; unfortunately it does not offer any micromechanical information of the healed areas in the defects.

In this study, electrochemical techniques were employed to understand the mechanism of corrosion protection, and to evaluate the self-healing performance of AVCs coated with IPDI-functionalized microcapsules. Fourier-transform infrared (FT-IR) spectroscopy was used to characterize the new IR absorption bands formed in the healed crevice after the treatment. Finally, the micromechanical behaviour of the self-healing products in the scratched crevice was also investigated by nanoindentation tests.

2. Experimental

2.1. Materials

Q235 steel was purchased from Shanghai BaoSteel. Alkyd varnish was purchased from Lehua Inc. China. The chemicals for the synthesis of the microcapsules were obtained from Sigma Aldrich

* Corresponding author at: State Key Laboratory for Marine Corrosion and Protection, Luoyang Ship Material Research Institute (LSMRI), 149-1 Zhuzhou Road, Laoshan District, Qingdao, 266101, PR China. Tel.: +86 532 68725174; fax: +86 532 68725001.
E-mail address: wwei020404@126.com (W. Wang).

0010-938X/$ - see front matter © 2013 Elsevier Ltd. All rights reserved.
http://dx.doi.org/10.1016/j.corsci.2013.11.050

and used as received. The water used in all the experiments was produced by a Millipore Milli-Q Plus 185 purification system and has a resistivity level higher than 18.1 MΩ cm.

2.2. Synthesis of IPDI microcapsules

IPDI microcapsules were synthesized with slight modification to our previously reported method [25]. In a typical procedure, under stirring (600 rpm), 6 g urea, 1 g ammonium chloride, and 1 g resorcinol were successively dissolved in 100 mL water. A 20 mL of 3.0 wt% aqueous solution of sodium dodecyl benzene sulfonate was added to the above mixture at room temperature. Then, 10 mL IPDI was slowly added into the mixture to form an oil-in-water microemulsion. After stirring for 30 min, pH of the emulsion was slowly adjusted to 3.5 by drop-wise addition of 0.05 M hydrochloric acid. One to two drops of 1-octanol were added to eliminate any surface bubbles. After that, 10 g of a 37 wt% aqueous solution of formaldehyde was added. The mixture was ultrasonicated for 10 min with a frequency of 20 kHz in an ice-bath. Finally, the temperature was raised to 55 °C at a rate of 1 °C min^{-1}. After 4 h of continuous stirring at 1000 rpm, the polymerized microcapsules were obtained, and they were repeatedly washed with ethanol and water to remove any residual impurities.

2.3. Preparation of AVC coating

Prior to all measurements, the Q235 steel samples (10 mm × 10 mm) were sealed by epoxy resin. The Q235 steel surface for tests was ground from 400 to 1200 grade SiC paper, respectively, and rinsed with double-distilled water. The prepared IPDI microcapsules were added into AVCs on surfaces of Q235 steel. The coatings were applied to the metal substrate with a thickness of 20 μm and 100 μm for scanning micro-reference electrode (SMRE) and electrochemical impedance spectroscopy (EIS) tests, respectively. Then, the samples were solidified at 40 °C for 48 h. The self-healing AVCs surface for tests was polished down to 1500 grade SiC paper (for SMRE experiments), then degreased ultrasonically in ethanol and acetone, and finally dried in air. Scratches on the coating were performed with a sharp doctor blade.

2.4. Experimental techniques

The morphologies of the microcapsules were acquired with a Hitachi S-4800 field emission scanning electron microscope (FE-SEM). The healed images of the scratched crevice were recorded with a VHX-1000 digital microscope (Keyence Co. Ltd). The chemical changes were investigated by FT-IR spectroscopy using a Thermo Scientific Nicolet iS10 spectrometer (Thermo Fisher Scientific Inc.), and the spectrum was recorded in 600–4000 cm^{-1} range. Nanoindentation tests were performed using Agilent G200 Nano-Indenter with a three-sided pyramidal diamond Berkovich indenter and continuous stiffness measurement (CSM) mode at a constant rate of 0.05 s^{-1} up to 3 m depth at 25 °C. The holding time of indentation was 10 s. The curve was measured three times with the same sample on the distinct surface regions at each indentation load.

The measurements of the potential distribution on the steel surface were recorded by SMRE technique using CSPM5500 scanning probe microscope system (Nano-Instruments, China). The scanning probe was prepared by one end of a Pt/Ir (10%) (0.1 mm) wire etched in a solution of 2 M sodium hydroxide with an alternating current to provide a tip with a diameter of 5 m. The scanning signal, with a micro reference electrode that was Ag/AgCl/KCl (saturated in water) with a potential of 0.197 V *vs.* NHE, was measured for 10 min during the probe scanning over a 2 mm × 2 mm area. The potential distributions over the whole test surface were presented as topographical 3D images. The EIS measurements were carried out using three-electrode cell, with a platinum counter electrode and a saturated calomel electrode as reference, which were conducted at a steady-state open circuit potential (OCP) disturbed with a perturbation of 20 mV rms on EG&G 2273 potentiostat. Furthermore, the criterion of EIS measurements under steady state condition was estimated that the fluctuation of OCP was ±2 mV within 600 s. The frequency range was from 10^5 Hz to 0.01 Hz, with 42 points. The corrosive electrolyte was 0.6 M NaCl solution, and all the tests were performed at 30 °C. Data were collected and fitted with different equivalent circuits using ZSimpwin software. The fitted results were judged by χ^2-value that was less than 10^{-3} for all the spectra, and the measured and simulated data were compared.

3. Results and discussion

3.1. SMRE studies on self-healing procedure

The FE-SEM overview morphology of the synthesized IPDI microcapsules via *in situ* polymerization is shown in Fig. 1. *In-situ* scanning over the entire area of a specimen helps to locate the active corrosion sites, and monitor the self-healing process in real time. The self-healing properties of the scratched coatings on a Q235 steel substrate surface immersed in a 0.005 M NaCl solution were studied by SMRE technique. The potential difference along the crevice shows the corrosion process. Each of the peaks in the potential distribution map represents an active pitting site in the scratched crevice [29]. A higher peak amplitude and wider peak distribution exhibit a stronger tendency towards localized corrosion [30]. A scratched line for the potential differences can be seen in the early immersion sample as shown in Fig. 2a. Several peaks (<30 mV) were observed in the beginning indicating localized corrosion in the scratched crevice. However, the potential difference changed significantly after 1 h (Fig. 2b). This result indicated that some of the IPDI molecules were released from the microcapsule cores over time, and they reacted with the water molecules on the substrate to produce water-insoluble products (polyurethanes) that then filled the scratched crevice. Consequently, the polyurethanes help in resisting the contact of the water with the Q235 substrate. Thus, the self-healing process effectively inhibited the progression of the metal corrosion process (Fig. 2c and d). The peaks of potential differences become much smaller after 4 h immersion (Fig. 2e). The heights of the pits along the scratched crevice apparently decreased with the progression in immersion time, thereby indicating that most pits along the crevice are continually

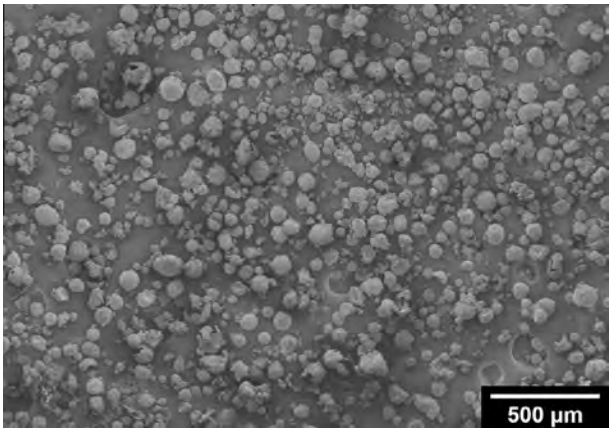

Fig. 1. FE-SEM overview image of IPDI microcapsules.

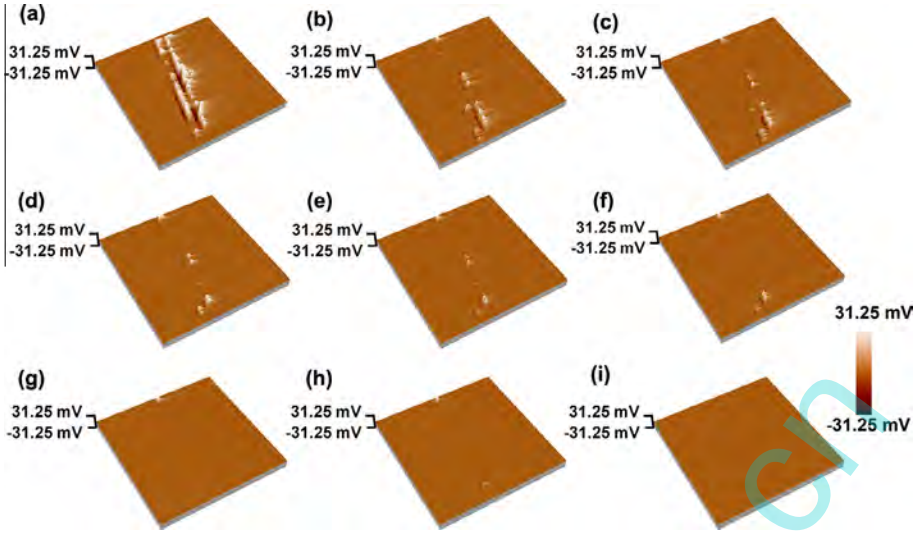

Fig. 2. Potential distributions above the scratched Q235 steel surface covered with IPDI-AVCs by SMRE (2×2 mm^2). (a–i), Correspond to 0.5, 1, 2, 3, 4, 5, 6, 7, and 8 h of immersion time in 0.005 M NaCl solution, respectively.

covered with more and more self-healing polyurethanes. There are only some weak potential difference peaks in the continuous process (Fig. 2f–g), and the peaks in the centre of the scanning map apparently disappeared. The self-healing process of the coating material eventually resulted in the disappearance of the largest potential difference peaks on the surface, and only a few peaks could be seen after 7 h immersion time (Fig. 2h). Finally, there are no potential difference peaks left in Fig. 2i indicating that the scratched crevice was entirely healed with self-healing products.

3.2. Chemical changes of self-healing process

The FT-IR analyses determined the chemical changes during the self-healing process in the healed crevice after water treatment. It is clearly seen in the optical image (Fig. 3a) that the scratched crevice are fully cured by the self-healing products after 100 h immersion in 0.6 M NaCl solution. The FT-IR spectra show the isocyanate (—NCO) peaks of IPDI molecules at 2259 and 1337 cm^{-1} (Fig. 3b-I). The conversion of isocyanate to urea in the product (polyurethane) was monitored by FT-IR, and the C—O and N—H stretching frequencies in the amide (CO—NH) were assigned at 1644 and 1558 cm^{-1} (Fig. 3b-II), respectively. Furthermore, polyurethanes deposited in the crevice (Area 1 in Fig. 3b-I) showed the stretching frequency of isocyanate groups at 2263 cm^{-1} (Fig. 3b-III). The FT-IR spectra of the AVCs (Area 2 in Fig. 3b-I) showed the stretching frequency of carbonyl (C=O) and methyl groups at 1732 and 2957 cm^{-1}, respectively (Fig. 3b-IV). New IR absorption bands due to the formation of urea groups appear at 3339 (N—H), 1644 (C=O), and 1558 (N—H) cm^{-1}. Thus, it could be spectroscopically proved that IPDI was responsible for the successful healing of the scratched crevice, and the entire crevice under this study contained polyurethanes as the self-healing water-insoluble products.

3.3. Micromechanical behaviour of self-healing products

The CSM technique can continuously measure the mechanical properties of materials without the need for discrete unloading cycles [20,31], and it can also be conducted at extremely small penetration depths. Thus, this technique is ideal for measuring micromechanical properties of the self-healing products in the scratched crevice of AVCs.

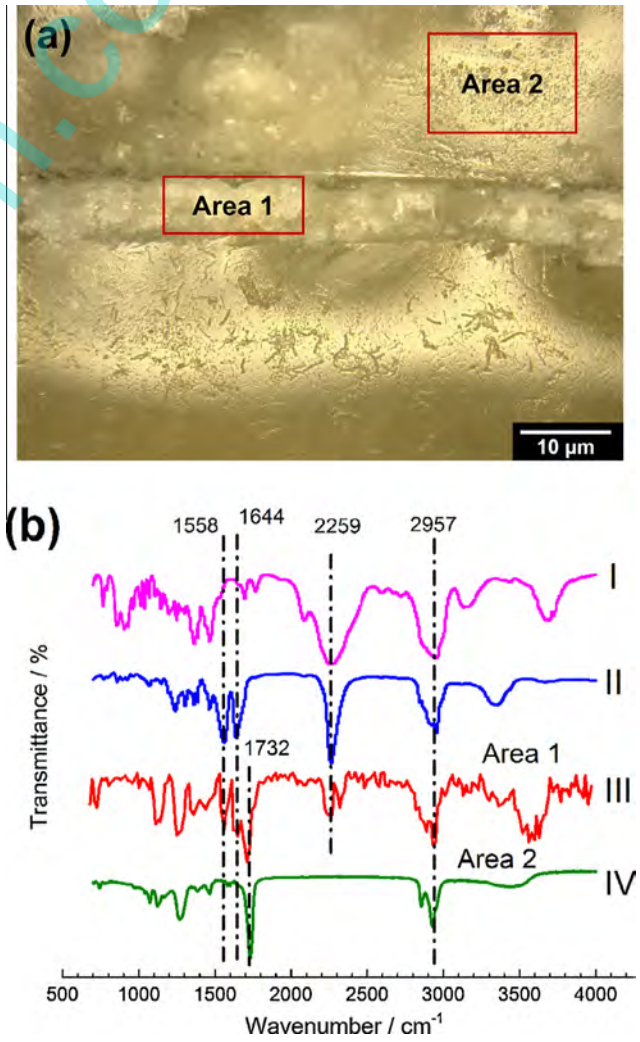

Fig. 3. (a) The AVC crevice on the Q235 substrate is filled with polyurethane, after 100 h immersion in 0.6 M NaCl solution; (b) FT-IR spectra of IPDI (I), polyurethane (II), polyurethane in the crevice of Area 1 (III), and AVCs of Area 2 (IV).

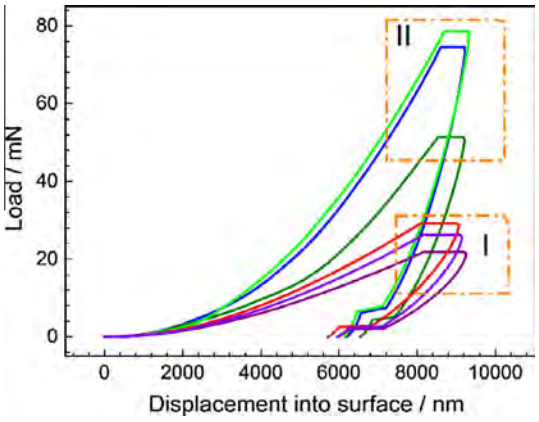

Fig. 4. Load–displacement curves of the AVCs (I) and polyurethane in AVC crevice (II) tested by using CSM. Each of the samples was measured three times on the distinct surface regions at each indentation load.

Fig. 4 shows the typical loading–unloading curves of AVCs (I) and the self-healing products in the scratched crevice (II). The average load during the holding time of the self-healing products was 68.178 mN, which was significantly higher than that of the AVCs at 25.786 mN. It proved that the self-healing products increased the loading force of the AVCs, thus successfully enhancing the scratched crevice's capability to endure outer stress. The average hardness and Young's modulus of the self-healing products (0.055 and 1.494 GPa, respectively) are relatively larger than those of the AVCs (0.020 and 0.670 GPa, respectively). These results indicate that the self-healing products enhanced both the Young's modulus and hardness of the AVCs. The loading portion of the nanoindentation with linear and nonlinear curves represents both elastic and plastic deformations [24,32]. Therefore, self-healing products are considerably more plastic in nature than the AVCs.

3.4. EIS measurements of self-healing process

EIS measurements could effectively monitor the self-healing process [33,34]. The total resistance combination of the Bode plot in EIS effectively showed the protective properties of the coating for the metal [35,36]. Fig. 5 gives the EIS results of the different self-healing process. In initial 20 h, Fig. 5a illustrates the occurrence of a pre-self-healing process that directly hindered the solution to penetrate into the bottom of the crevice, because the two side walls of the scratched crevice touched each other due to AVC's inherent elasticity. Thus, the phase angle spectra (Fig. 5b) reveals three time constants ascribed to the coating formed by the two side walls of the scratched crevice touched each other, the AVCs and the double layer, respectively. Moreover, some left-over AVC materials also slowed down the penetration of NaCl solution, within 20 h after the scratch was made on the substrate. The Bode plots in Fig. 5e, h, and k reveal two time constants: one in the middle frequency range due to the self-healing coating, and a second one in the low frequency range that can be ascribed to the response of processes occurring at the coating/substrate interface [37]. The rising trend of phase angle curves in the middle frequency range (Fig. 5b, e and h) indicates that the resistance of the AVCs is enhanced by the self-healing process. It can be seen the capacitive response in the middle frequency range and the corresponding resistive response in the low frequency range due to the self-healing coating protection [38]. Furthermore, in the coating failure process, the Nyquist plot in Fig. 5j displays similar capacitive loops in the high frequency range and a Warburg impedance in the low frequency range.

Impedance modulus ($|Z|$) at a frequency of 0.01 Hz of each Bode plot is used to evaluate the coating resistance in Fig. 6. Four typical stages of the impedance modulus value ($f = 0.01$ Hz) in the curve could be easily distinguished. The $|Z|$ value of the AVC coating in this process is adjusted as shown in Fig. 6-I. As shown in Fig. 6-II, the increasing trend of the $|Z|$ value (from 0.782 to 1.515 MΩ cm^2) indicates that the solution penetrates into the mouth of the crevice, where water reacts with isocyanate groups and triggers the inflow of self-healing materials (IPDI) from the microcapsules. Consequently, more and more healing materials are produced over time, and these water-insoluble reaction products get filled in at the bottom and walls of the crevice. The $|Z|$ value reaches the maximum peak value 1.548 MΩ cm^2 after 96 h of immersion. Then, the $|Z|$ value started a decreasing trend, from 1.406 to 0.675 MΩ cm^2 in Part III of the curve, with little fluctuation that demonstrates the slightly on-going self-healing process and water penetration. Since the scratch now has some micro crevices, the solution can slowly continue to penetrate into the healed crevice down to the metal bottom surface, and the healing process is repeated until the reaction is completed and so the healing materials are exhausted after 406 h of immersion time. Finally, the AVC loses the self-healing ability as $|Z|$ value becomes lower than 0.092 MΩ cm^2, and therefore cannot anymore resist the solution penetration (IV). The Nyquist plots for such coating failures are shown in Fig. 5g and h. Different self-healing stages are obviously distinguished from each other in the self-healing process. These results obtained clearly confirmed that a physical barrier had formed in the self-healing process, thereby empowering the AVCs with significant protective ability.

The complex pre-self-healing process included the water penetration, two side walls of the scratched crevice touched each other, and self-healing process of IPDI. Thus, the first equivalent circuit (Fig. 7a) was used to fit the EIS data of the scratched AVCs in the pre-self-healing process in 0.6 M NaCl solution. Further, the second equivalent circuit (Fig. 7b) was used to fit the EIS data of the scratched AVCs in the self-healing process and water penetration in 0.6 M NaCl solution, whereas the third one (Fig. 7c) was used to fit the EIS data of coating failure displaying a Warburg impedance. R_s is the solution resistance of NaCl solution. R_e and C_e represent the resistance and capacitance of the AVC's inherent elasticity. R_c and Q_c represent the coating resistance and capacitance of scratched AVCs. R_{ct} and Q_{dl} represent the metal charge transfer resistance and double layer capacitance. C_c and C_{dl} represent the capacitance of scratched AVCs and the metal double layer capacitance in the pre-self-healing process. Z_w represents Warburg diffusion coefficient. For the capacitive loops, the coefficients n_c and n_{dl} represent a depressed feature in the Nyquist diagram.

The coating resistance R_c of the scratched AVCs, which came from the fitting results of the experimental EIS, were plotted in Fig. 8a. During immersion the values of the R_c had the same trend of $|Z|$ values (Fig. 6). According to the fitting results in Table 1, the decreasing trend of the R_c value (from 0.503 to 0.307 MΩ cm^2) indicates that the solution slowly penetrates into the bottom of the crevice in the pre-self-healing process. However, the increasing trend of the R_c value (from 0.103 to 1.307 MΩ cm^2) in Table 2 indicates that the self-healing process enhances the barrier of the scratched crevice in AVCs. After immersion for 96 h, the R_c value gradually decreased, indicating that the barrier of the AVCs was gradually deteriorated by water penetration. Finally, the AVC loses the self-healing ability as R_c value becomes lower than 0.0702 MΩ cm^2 (Fig. 8a). The constant phase element of the coating Q_c was plotted in Fig. 8b. The values of Q_c were gradually decreasing (from 7.603 to 0.331 μF cm^{-2}) before 209 h. However, the values of Q_c were gradually increasing (from 0.331 to

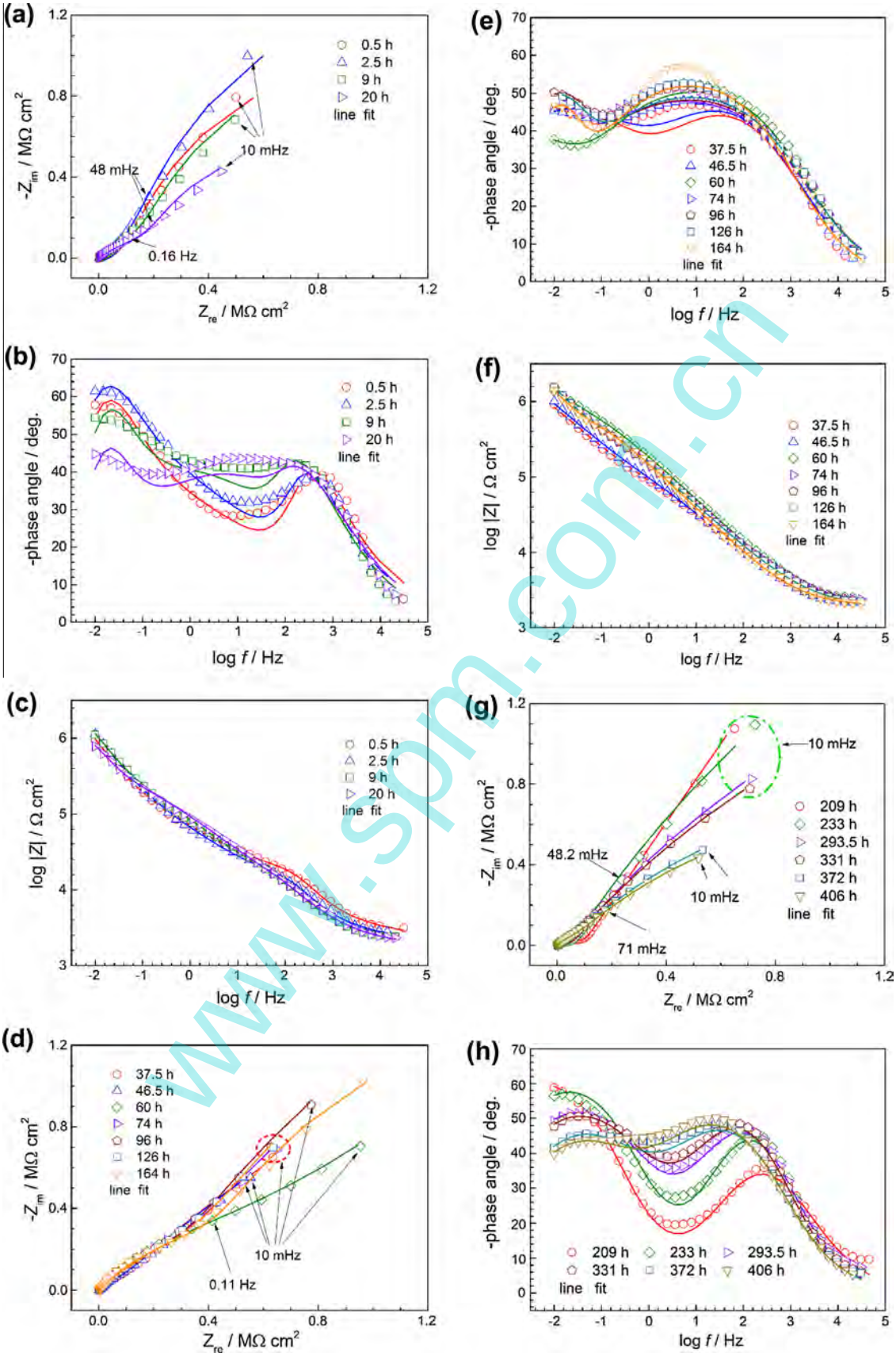

Fig. 5. Nyquist and Bode plots of Q235 (1 cm × 1 cm) coated with IPDI-AVC with a 0.5 cm length scratch. Different stages of the self-healing process: pre-self-healing process (a, b and c), self-healing process (d, e and f), water penetration (g, h and i), and coating failure (j, k and l).

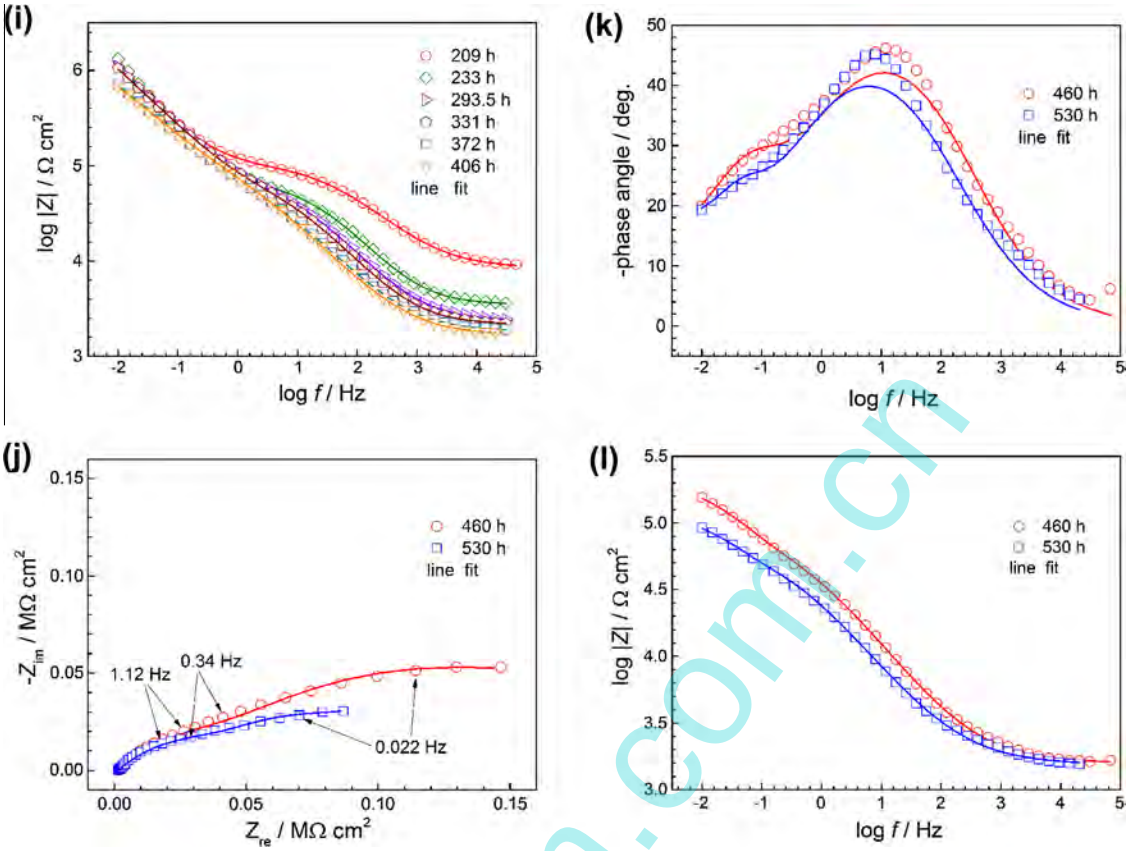

Fig. 5 (*continued*)

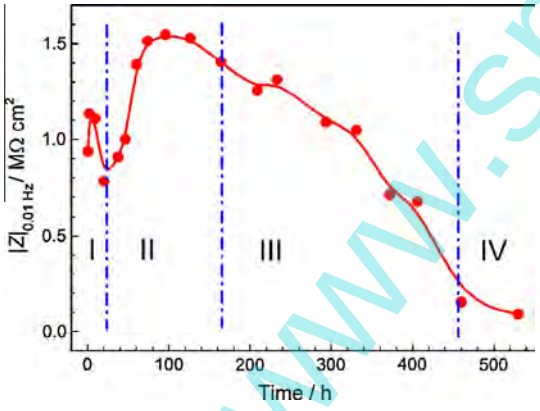

Fig. 6. Impedance modulus (f = 0.01 Hz) of the scratched AVCs in 0.6 M NaCl solution.

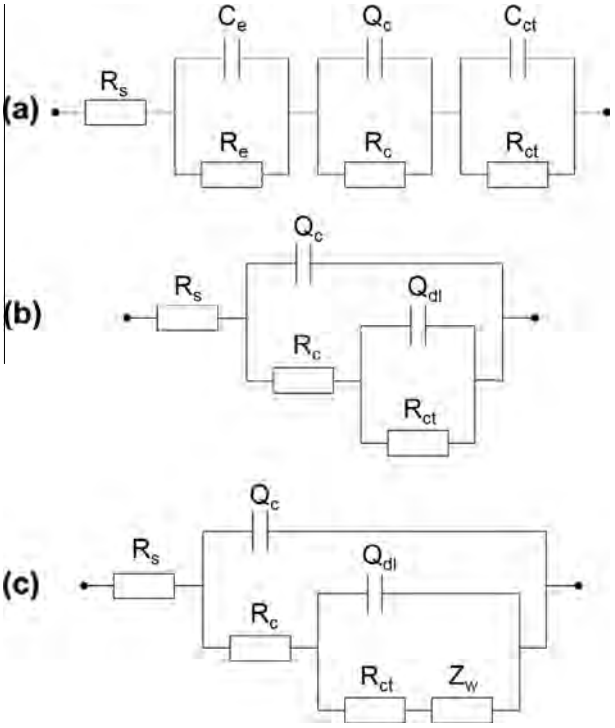

Fig. 7. Equivalent circuit models used to fit the experiment impedance data of scratched AVCs in 0.6 M NaCl solution.

2.653 μF cm^{-2}) with slight fluctuations during immersion 406 h. After immersion for 406 h, the healed crevice in AVCs started to fail.

The reciprocals of charge-transfer resistance, $1/R_{ct}$, and the constant phase element of double layer capacitance, Q_{dl}, are plotted in Fig. 9a and b, respectively. The $1/R_{ct}$ values are used to represent the corrosion rate of steel in different environments [39]. The lower is the value of $1/R_{ct}$ for the coating; the greater is the corrosion resistance of the AVCs [40]. Thus, the values of $1/R_{ct}$ in the self-healing process of stages I, II, and III in Fig. 6 are lower than 0.987 MS cm^{-2}; whereas the value for IV stage is higher than 32.916 MS cm^{-2} in stage IV. Furthermore, the values of Q_{dl} slightly fluctuated (between 3.789 and 3.126 μF cm^{-2}) in the self-healing process, indicating that the on-going self-healing process hindered the water penetration. Then, the values of Q_{dl} slightly fluctuated

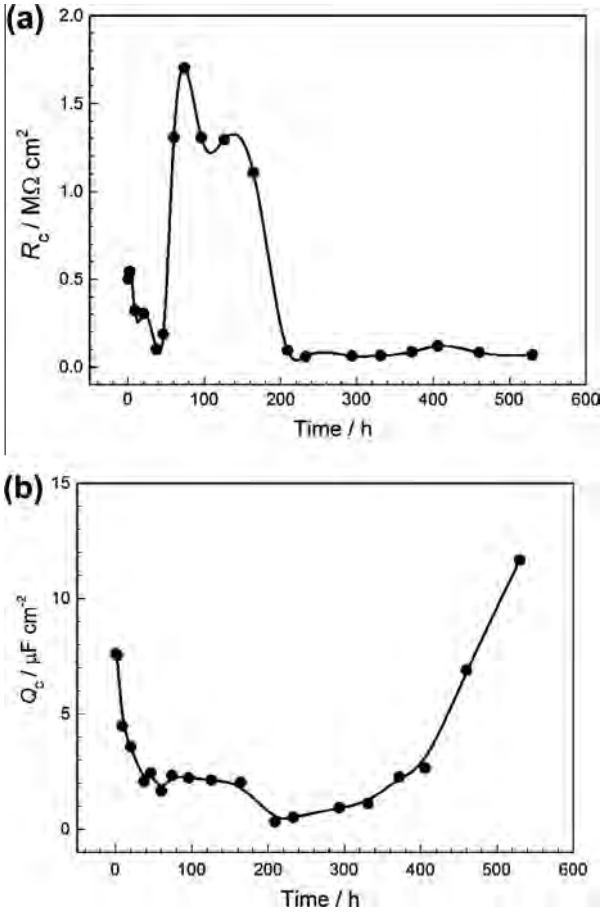

Fig. 8. The changes in the coating resistance R_c (a) and the coating capacitance Q_c (b) of scratched AVCs in 0.6 M NaCl solution.

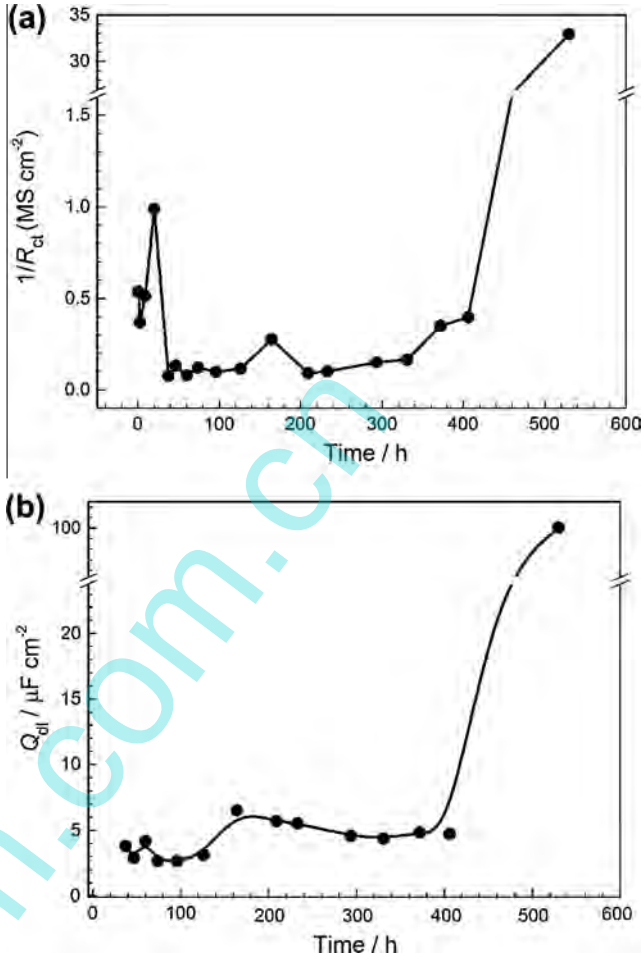

Fig. 9. The change in the reciprocals of charge-transfer resistance $1/R_{ct}$ (a) and the double layer capacitance Q_{dl} of (b) scratched AVCs in 0.6 M NaCl solution.

Table 1
Electrochemical parameters of scratched AVCs in the pre-self-healing process.

Time (h)	R_e (kΩ cm^2)	C_e (μF cm^{-2})	Q_c (μF cm^{-2})	n_c	R_c (MΩ cm^2)	C_{dl} (μF cm^{-2})	R_{ct} (MΩ cm^2)
0.5	9.291	0.0955	7.603	0.421	0.503	18.650	1.860
2.5	6.871	0.161	7.558	0.454	0.544	15.470	2.703
9	5.883	0.340	4.487	0.525	0.322	14.440	1.947
20	3.247	0.550	3.563	0.531	0.307	21.970	1.013

Table 2
Electrochemical parameters of scratched AVCs in the last three self-healing processes.

Time (h)	Q_c (μF cm^{-2})	n_c	R_c (MΩ cm^2)	Q_{dl} (μF cm^{-2})	n_{dl}	R_{ct} (MΩ cm^2)	Z_w (Ω cm^2)
37.5	2.058	0.613	0.103	3.789	0.546	13.180	–
46.5	2.438	0.592	0.187	2.898	0.584	7.561	–
60	1.656	0.598	1.308	4.173	0.630	12.620	–
74	2.328	0.564	1.703	2.662	0.950	8.228	–
96	2.227	0.573	1.307	2.647	0.919	10.120	–
126	2.126	0.580	1.296	3.126	0.922	8.659	–
164	2.024	0.619	1.109	6.505	1.000	3.619	–
209	0.331	0.637	0.0960	5.685	0.709	10.700	–
233	0.507	0.729	0.0599	5.517	0.721	9.858	–
293.5	0.927	0.701	0.0645	4.579	0.654	6.619	–
331	1.118	0.704	0.0662	4.368	0.638	6.029	–
372	2.263	0.656	0.0865	4.826	0.600	2.857	–
406	2.653	0.648	0.121	4.725	0.589	2.516	–
460	6.890	0.596	0.0830	26.811	0.783	0.107	0.000182
530	11.670	0.577	0.0702	100.100	1.000	0.0304	0.000191

(between 5.685 and 4.725 μF cm^{-2}) during water penetration, following with the Q_{dl} increasing to 100.1 μF cm^{-2} at the coating failure stage.

Thus, the entire self-healing process of AVCs was well monitored by EIS, and four different self-healing stages were clearly distinguished as follows: (I) pre-self-healing process, (II) self-healing process, (III) water penetration, and (IV) coating failure.

4. Conclusion

The AVCs fabricated with IPDI microcapsules react with water when immersed in it, and are proved to be well capable of physically healing the coating defects in case of a damage to the surface. The SMRE results evidently showed the protective ability of the modified AVCs by a self-healing phenomenon that triggers by water immersion, thereby hindering the corrosion process at the damaged area in the coating. The formation of new IR absorption bands in the healed crevice, confirmed that IPDI successfully produced water-insoluble polyurethanes as the self-healing products. Furthermore, the self-healing products could also bear much higher loading force than the AVCs itself indicating that they are significantly more plastic in nature than the AVCs. The entire self-healing process of IPDI-AVCs was initiated by corrosion activities, which could be well monitored by EIS, and four different self-healing stages were clearly distinguished (e.g., pre-self-healing process, self-healing process, water penetration, and coating failure).

Acknowledgment

This research was supported by China Postdoctoral Science Foundation (No. 2013M531686).

References

[1] E.B. Murphy, F. Wudl, The world of smart healable materials, Prog. Polym. Sci. 35 (2010) 223–251.
[2] L. Yuan, G.Z. Liang, J.Q. Xie, L. Li, J. Guo, Preparation and characterization of poly(urea-formaldehyde) microcapsules filled with epoxy resins, Polymer 47 (2006) 5338–5349.
[3] M.M. Caruso, D.A. Davis, Q. Shen, S.A. Odom, N.R. Sottos, S.R. White, J.S. Moore, Mechanically-induced chemical changes in polymeric materials, Chem. Rev. 109 (2009) 5755–5798.
[4] M. Huang, H. Zhang, J. Yang, Synthesis of organic silane microcapsules for self-healing corrosion resistant polymer coatings, Corros. Sci. 65 (2012) 561–566.
[5] Q. Li, A.K. Mishra, N.H. Kim, T. Kuila, K.T. Lau, J.H. Lee, Effects of processing conditions of poly(methylmethacrylate) encapsulated liquid curing agent on the properties of self-healing composites, Composites: Part B 49 (2013) 6–15.
[6] J.F. Su, J. Qiu, E. Schlangen, Stability investigation of self-healing microcapsules containing rejuvenator for bitumen, Polym. Degrad. Stab. 98 (2013) 1205–1215.
[7] X.M. Tong, M. Zhang, M.S. Wang, Y. Fu, Effects of surface modification of self-healing poly(melamine-urea-formaldehyde) microcapsules on the properties of unsaturated polyester composites, J. Appl. Polym. Sci. 127 (2013) 3954–3961.
[8] A. Fereidoon, M.G. Ahangari, M. Jahanshahi, Effect of nanoparticles on the morphology and thermal properties of self-healing poly(urea-formaldehyde) microcapsules, J. Polym. Res. 20 (2013) 151.
[9] S.H. Cho, S.R. White, P.V. Braun, Self-healing polymer coatings, Adv. Mater. 20 (2008) 1–5.
[10] S. Billiet, X.K.D. Hillewaere, R.F.A. Teixeira, F.E. Du Prez, Chemistry of crosslinking processes for self-healing polymers, Macromol. Rapid Commun. 34 (2013) 290–309.
[11] H.H. Jin, G.M. Miller, S.J. Pety, A.S. Griffin, D.S. Stradley, D. Roach, N.R. Sottos, S.R. White, Fracture behavior of a self-healing, toughened epoxy adhesive, Int. J. Adhes. Adhes. 44 (2013) 157–165.
[12] Y. González-García, S.J. García, A.E. Hughes, J.M.C. Mol, A combined redox-competition and negative-feedback SECM study of self-healing anticorrosive coatings, Electrochem. Commun. 13 (2011) 1094–1097.
[13] A. Yabuki, T. Nishisaka, Self-healing capability of porous polymer film with corrosion inhibitor inserted for corrosion protection, Corros. Sci. 53 (2011) 4118–4123.
[14] G. Williams, S. Geary, H.N. McMurray, Smart release corrosion inhibitor pigments based on organic ion-exchange resins, Corros. Sci. 57 (2012) 139–147.
[15] S.A.S. Dias, S.V. Lamaka, C.A. Nogueira, T.C. Diamantino, M.G.S. Ferreira, Sol–gel coatings modified with zeolite fillers for active corrosion protection of AA2024, Corros. Sci. 62 (2012) 153–162.
[16] Y.K. Song, Y.H. Jo, Y.J. Lim, S.Y. Cho, H.C. Yu, B.C. Ryu, S.I. Lee, C.M. Chung, Sunlight-induced self-healing of a microcapsule-type protective coating, ACS Appl. Mater. Interfaces 5 (2013) 1378–1384.
[17] M. Kouhi, A. Mohebbi, M. Mirzaei, M. Peikari, Optimization of smart self-healing coatings based on micro/nanocapsules in heavy metals emission inhibition, Prog. Org. Coat. 76 (2013) 1006–1015.
[18] J. Yang, M.W. Keller, J.S. Moore, S.R. White, N.R. Sottos, Microencapsulation of isocyanates for self-healing polymers, Macromolecules 41 (2008) 9650–9655.
[19] M.X. Huang, J.L. Yang, Facile microencapsulation of HDI for self-healing anticorrosion coatings, J. Mater. Chem. 21 (2011) 11123–11130.
[20] D.A. Lucca, K. Herrmann, M.J. Klopfstein, Nanoindentation: measuring methods and applications, CIRP Ann. – Manuf. Technol. 59 (2010) 803–819.
[21] I.A. Kartsonakis, E.P. Koumoulos, A.C. Balaskas, G.S. Pappas, C.A. Charitidis, G.C. Kordas, Hybrid organic–inorganic multilayer coatings including nanocontainers for corrosion protection of metal alloys, Corros. Sci. 57 (2012) 56–66.
[22] Y.H. Chu, H.J. Li, Q.G. Fu, L.H. Qi, L. Li, Bamboo-shaped SiC nanowire-toughened SiC coating for oxidation protection of C/C composites, Corros. Sci. 70 (2013) 11–16.
[23] D. Gopi, E. Shinyjoy, M. Sekar, M. Surendiran, L. Kavitha, T.S. Sampath Kumar, Development of carbon nanotubes reinforced hydroxyapatite composite coatings on titanium by electrodeposition method, Corros. Sci. 73 (2013) 321–330.
[24] J. Lee, M.Q. Zhang, D. Bhattacharyya, Y.C. Yuan, K. Jayaraman, Y.W. Mai, Micromechanical behaviour of self-healing epoxy and hardener-loaded microcapsules by nanoindentation, Mater. Lett. 76 (2012) 62–65.
[25] W. Wang, L. Xu, F. Liu, X. Li, L. Xing, Synthesis of isocyanate microcapsules and micromechanical behaviour improvement of microcapsule shells by oxygen plasma treated carbon nanotubes, J. Mater. Chem. A 1 (2013) 776–782.
[26] J.D. Rule, E.N. Brown, N.R. Sottos, S.R. White, J.S. Moore, Wax-protected catalyst microspheres for efficient self-healing materials, Adv. Mater. 17 (2005) 205–208.
[27] H. Jin, G.M. Miller, N.R. Sottos, S.R. White, Fracture and fatigue response of a self-healing epoxy adhesive, Polymers 52 (2011) 1628–1634.
[28] H. Jin, G.M. Miller, S.J. Pety, A.S. Griffin, D.S. Stradley, D. Roach, N.R. Sottos, S.R. White, Fracture behavior of a self-healing, toughened epoxy adhesive, Int. J. Adhes. Adhes. 44 (2013) 157–165.
[29] H. Xu, Y. Liu, W. Chen, R.G. Du, C.J. Lin, Corrosion behaviour of reinforcing steel in simulated concrete pore solutions: a scanning micro-reference electrode study, Electrochim. Acta 54 (2009) 4067–4072.
[30] N. Cui, H.Y. Ma, J.L. Luo, S. Chiovelli, Use of scanning reference electrode technique for characterizing pitting and general corrosion of carbon steel in neutral media, Electrochem. Commun. 3 (2001) 716–721.
[31] X. Li, B. Bhushan, A review of nanoindentation continuous stiffness measurement technique and its applications, Mater. Charact. 48 (2002) 11–36.
[32] M. Tehrani, M. Safdari, M.S. Al-Haik, Nanocharacterization of creep behaviour of multiwall carbon nanotubes/epoxy nanocomposite, Int. J. Plast. 27 (2011) 887–901.
[33] J.B. Jorcin, G. Scheltjens, Y. Van Ingelgem, E. Tourwé, G. van Assche, I. de Graeve, B. van Mele, H. Terryn, A. Hubin, Investigation of the self-healing properties of shape memory polyurethane coatings with the 'odd random phase multisine' electrochemical impedance spectroscopy, Electrochim. Acta 55 (2010) 6195–6203.
[34] K.Y. Zhang, L.D. Wang, G.C. Liu, Copper(II) 8-hydroxyquinolinate 3D network film with corrosion inhibitor embedded for self-healing corrosion protection, Corros. Sci. 75 (2013) 38–46.
[35] G.W. Walter, A review of impedance plot methods used for corrosion performance analysis of painted metals, Corros. Sci. 26 (1986) 681–703.
[36] I.A. Kartsonakis, A.C. Balaskas, E.P. Koumoulos, C.A. Charitidis, G.C. Kordas, Incorporation of ceramic nanocontainers into epoxy coatings for the corrosion protection of hot dip galvanized steel, Corros. Sci. 57 (2012) 30–41.
[37] I.A. Kartsonakis, A.C. Balaskas, E.P. Koumoulos, C.A. Charitidis, G. Kordas, Evaluation of corrosion resistance of magnesium alloy ZK10 coated with hybrid organic–inorganic film including containers, Corros. Sci. 65 (2012) 481–493.
[38] W. Trabelsi, E. Triki, L. Dhouibi, M.G.S. Ferreira, M.L. Zheludkevich, M.F. Montemor, The use of pre-treatment based on doped silane solutions for improved corrosion resistance of galvanised steel substrates, Surf. Coat. Technol. 200 (2006) 4240–4250.
[39] W.J. Lorenz, F. Mansfeld, Determination of corrosion rates by electrochemical DC and AC methods, Corros. Sci. 21 (1981) 641–672.
[40] Y. Shao, H. Huang, T. Zhang, G. Meng, F. Wang, Corrosion protection of Mg–5Li alloy with epoxy coatings containing polyaniline, Corros. Sci. 51 (2009) 2906–2915.